Korean J. Chem. Eng., **31**(9), 1553-1563 (2014)
DOI: 10.1007/s11814-014-0123-2

pISSN: 0256-1115
eISSN: 1975-7220

CO_2 reforming of methane over Ni-Cu/Al_2O_3-ZrO_2 nanocatalyst : The influence of plasma treatment and process conditions on catalytic properties and performance

Nader Rahemi*,, Mohammad Haghighi*,**,†, Ali Akbar Babaluo*,***, Mahdi Fallah Jafari****, and Somaiyeh Allahyari*,****

*Chemical Engineering Faculty, Sahand University of Technology, P. O. Box 51335-1996, Sahand New Town, Tabriz, Iran
**Reactor and Catalysis Research Center (RCRC), Sahand University of Technology, P. O. Box 51335-1996, Sahand New Town, Tabriz, Iran
***Nanostructure Material Research Center (NMRC), Sahand University of Technology, P. O. Box 51335-1996, Sahand New Town, Tabriz, Iran
****National Iranian Oil Refining & Distribution Company (NIORDC), National Iranian Oil Company (NIOC), P. O. Box 15815-3499, Tehran, Iran
(*Received 20 December 2013 • accepted 21 April 2014*)

Abstract−Argon glow discharge plasma was applied for treatment of impregnated Ni-Cu/Al_2O_3-ZrO_2 nanocatalyst. The catalytic performance toward CO_2 reforming of methane and the physicochemical properties were investigated by means of GC, BET, XRD, FESEM, TEM, EDX, TG-DTG, XPS and FTIR techniques. The plasma-treated nanocatalyst contains smaller crystal size and high dispersion of NiO. Plasma treatment decreased particle size and plasma high energy species flattened particles on support, increasing the interaction between support and active metals which leads to high catalytic activity. Low temperature activity and H_2/CO ratio closer to 1 was observed for plasma-treated nanocatalyst compared to non-treated sample. Moreover, higher product yield and H_2/CO ratio was found in CH_4/CO_2=1 rather than CH_4/CO_2=1.5. Time on stream test during 1,440 min at 850 °C showed plasma-treated Ni-Cu/Al_2O_3-ZrO_2 nanocatalyst did not experience any deactivation in terms of CH_4 and CO_2 conversion and H_2/CO ratio.

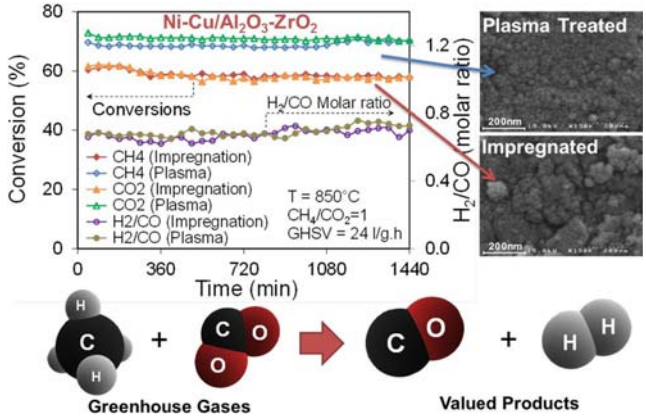

Keywords: Syngas, Dry Reforming, Ni-Cu/Al_2O_3-ZrO_2, Non-thermal Plasma

INTRODUCTION

Recently, carbon dioxide reforming of methane to synthesis gas has received a great deal of attention [1-7]. This process converts two undesirable greenhouse gases into valuable products, whereas the low H_2/CO ratio obtained in this process is suitable for further synthesis of hydrocarbons [8,9]. Another advantage of carbon dioxide reforming of methane is its capability in utilization of biogas and natural gas with large amounts of CO_2 [10,11].

The main reaction in dry reforming of methane is:

$$CH_4+CO_2 \rightarrow 2CO+2H_2 \qquad \Delta H^o_{298}=+247 \text{ kJ/mol.} \qquad (1)$$

While the reverse water gas shift reaction (RWGS (2)), the Boudouard reaction (3) and methane decomposition (4), are the side reactions as follows:

$$H_2+CO_2 \rightarrow H_2O+CO \qquad \Delta H^o_{298}=+39.5 \text{ kJ/mol.} \qquad (2)$$

$$2CO \leftrightarrow CO_2+C \qquad \Delta H^o_{298}=-171 \text{ kJ/mol.} \qquad (3)$$

$$CH_4 \leftrightarrow 2H_2+C \qquad \Delta H^o_{298}=75 \text{ kJ/mol.} \qquad (4)$$

Nickel-based catalysts have been widely used in carbon dioxide reforming of methane. However, the Boudouard reaction and the methane decomposition reaction suffer from low catalytic activity and instability against coke deposition [12]. In recent years, to im-

†To whom correspondence should be addressed.
E-mail: haghighi@sut.ac.ir

prove the catalytic performance of nickel-based catalysts, a number of new catalyst preparation and treatment methods have emerged [6,13,14]. Among these, plasma treatment, as a special kind of energy donation, is an effective method for catalyst preparation and its modification under non equilibrium conditions [15]. Glow discharge plasma, a kind of non-thermal plasma, has shown broad application prospects in improving metal dispersion, modulating the interaction between active components and carrier, synthesis of ultrafine catalyst particles, as well as surface modifications [12]. Cheng et al. [16] found a high dispersion of active species over support and a better stability for Ni/Al_2O_3 after a glow discharge plasma treatment. Zhang et al. [17] indicated that non thermal plasma may lead to produce Ni/Al_2O_3 catalyst with lower temperature activity and an enhanced stability for CO_2 reforming of methane. Zou et al. [18] reported a special metal-support interface for Ni based catalysts after argon glow discharge plasma. It has been proven that the nature of support [19,20] and the presence of promoters [21-24] can enhance physicochemical properties, catalytic activity and stability of Ni/Al_2O_3 catalyst. Choi et al. [25] studied the performance of Ni/Al_2O_3 catalysts promoted by addition of Co, Cu, Zr, Mn, Mo, Ti, Ag and Sn. Only Co, Cu and Zr showed a slight improvement in activity, compared to the conventional catalyst, while the rest of the additives reduced the activity in dry reforming. Dong et al. showed that Cu had a better NiO dispersion in comparison with Co and Fe [26].

Our group at Reactor and Catalysis Research Center has done systematic research on plasma-treated catalysts to introduce the best Ni-based catalyst for CO_2 reforming of methane. At the first part of the research for Ni/Al_2O_3 catalysts, the effect of support promoters like CeO_2 [27], ZrO_2 [28] and MgO [29] and active phase promoters like cobalt [30] and copper [31] has been investigated. From this part of the investigation, we have addressed that ZrO_2 and cobalt are the better support and active phase promoters, respectively. Then we reported the simultaneous promotion of cobalt and ZrO_2 in plasma-treated catalyst [32]. In the next part of the research we focused on the effect of calcination temperature [33] and effect of Ni loading in selected $Ni\text{-}Co/Al_2O_3\text{-}ZrO_2$ catalyst. NiO size reduction, improvement in dispersion, surface enrichment of active phase, low temperature activity and stability against coke deposition have been observed in all mentioned plasma-treated samples rather than impregnated catalysts. In the present paper and continuing research in our research center, we explored the effect of argon glow discharge plasma on reactivity, stability and structural properties of simultaneous Cu and ZrO_2 promoted Ni/Al_2O_3 nanocatalyst in CO_2 reforming of methane. The impregnated $Ni\text{-}Cu/Al_2O_3\text{-}ZrO_2$ nanocatalyst has been treated with plasma and characterized by XRD, FESEM, TEM, BET, TG-DTG, FTIR and XPS analysis. In addition, the effect of operating temperature, feed composition and gas hourly space velocity (GHSV) on the feed conversion, product yield and H_2/CO ratio have been investigated. To study nanocatalyst activity in long-term use, a stability test has been performed for plasma-treated and non-treated $Ni\text{-}Cu/Al_2O_3\text{-}ZrO_2$ nanocatalysts.

MATERIALS AND METHODS

1. Materials

In this work nickel nitrate hexahydrate ($Ni(NO_3)_2\cdot 6H_2O$) and copper nitrate hexahydrate ($Cu(NO_3)_2\cdot 6H_2O$) were used as nickel and copper precursors, respectively, and $\gamma\text{-}Al_2O_3$ powder was used as support. All reagents were purchased from Merck Company and used without further purification. Methane and carbon dioxide (feed gas), hydrogen (reducing gas) and argon as plasma forming gas with high purity, purchased from Technical Gas Services in Ajman, UAE.

2. Nanocatalyst Preparation and Procedures

Fig. 1 illustrates a schematic flowchart of the preparation steps of $Ni\text{-}Cu/Al_2O_3\text{-}ZrO_2$ nanocatalyst using non-thermal plasma (NCAZ-P). For synthesis of $Ni\text{-}Cu/Al_2O_3\text{-}ZrO_2$ nanocatalyst, nickel and copper were added simultaneously to $Al_2O_3\text{-}ZrO_2$ support. A mixture of ($Ni(NO_3)_2\cdot 6H_2O$), ($Cu(NO_3)_2\cdot 6H_2O$) and $Al_2O_3\text{-}ZrO_2$ was prepared using an appropriate loadings of Cu (3%) and Ni (10%). The aqueous mixture was stirred for 5 h at 60 °C. The resultant mixture was dried for 8 h at 120 °C under air flow condition. The dried nanocatalyst was exposed to glow discharge plasma before calcination. A schematic flow chart of the glow discharge plasma experimental setup for treatment of $Ni\text{-}Cu/Al_2O_3\text{-}ZrO_2$ nanocatalysts is illustrated in Fig. 2.

The plasma reactor was made of glass (i.d. 50 mm), and the dis-

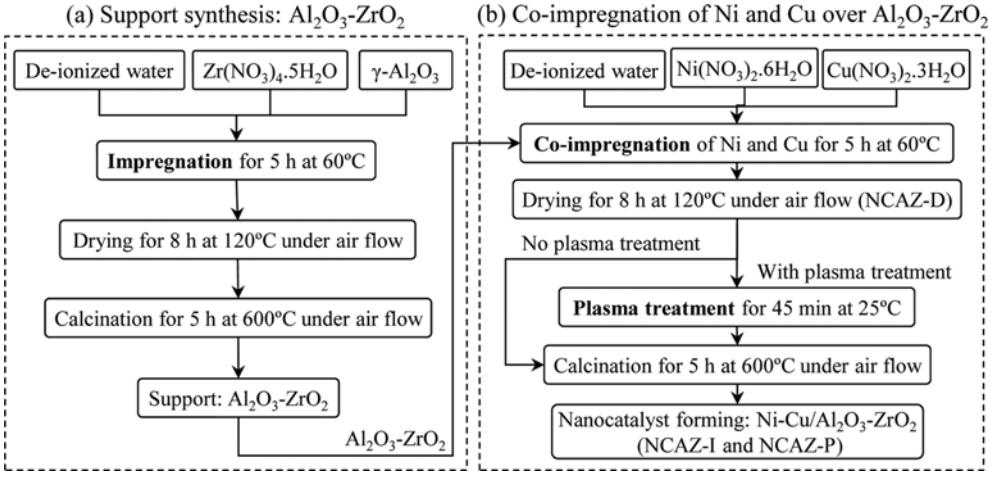

Fig. 1. Schematic flow chart for the preparation steps of $Ni\text{-}Cu/Al_2O_3\text{-}ZrO_2$ nanocatalyst via impregnation of ZrO_2, Ni and Cu over Al_2O_3 and non-thermal plasma treatment.

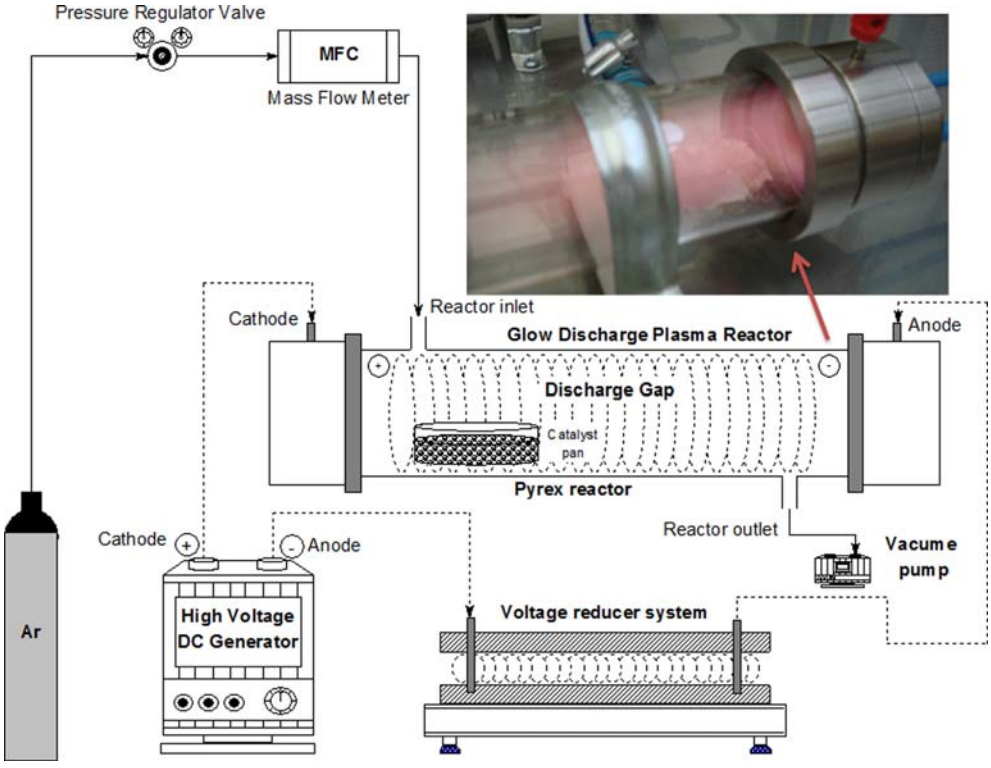

Fig. 2. Schematic flow chart of non-thermal plasma experimental setup for treatment of Ni-Cu/Al_2O_3 nanocatalyst.

tance between positive and negative electrodes was fixed at 200 mm. To generate the required power for glow discharge plasma, a DC high voltage generator was applied. The generated voltage was ca. 1,000 V. To remove impurities, the reactor was washed with deionized water and acetone. As it is shown in Fig. 2, 0.2 gr of dried nanocatalyst (NCAZ-D) was loaded on a quartz plate in the positive column and was moisturized by two or three droplets of distilled water. To form glow discharge plasma, it is necessary to use a vacuum pump. In our research the initial pressure was 10^{-3} torr using a turbomolecular vacuum pump (Pfeiffer). The reactor was purged by plasma forming gas (Argon). The current was 100 mA and when pressure reached to 100-200 Pa, the plasma was formed clearly. Ni-Cu/Al_2O_3-ZrO_2 sample was put in plasma environment for 15 min and the treatment was repeated three times to get a uniformly treated powder. In the next step, the sample was calcined at 600 °C for 5 h under air flow condition. The obtained powder (NCAZ-P) was finally shaped into cylindrical species (1 mm in diameter, 2 mm in height). For synthesis of impregnated Ni-Cu/Al_2O_3-ZrO_2 nanocatalyst (NCAZ-I), after drying, the sample was put in the furnace to be calcined for 5 h at 600 °C under air flow condition.

3. Nanocatalyst Characterization Techniques

The structural characteristics of nanocatalysts were examined by using X-ray diffraction patterns in 2θ range from 20° to 90° and scanning rate of 0.02°/s by a Siemens diffractometer D5000 with monochromatized Cu-Kα (λ=1.54178 Å) radiation at 30 mA and 40 kV. The phase identification was made by comparison to Joint Committee on Powder Diffraction Standards (JCPDSs). Microstructure, particle size and morphology were investigated by field emission scanning electron microscopy (HITACHI S-4160). To detect active phase particles and their dispersion on support, transmission electron microscopy (TEM) was carried out on a VEGA\\TESCAN, BSE DETECTOR. The specific surface area (BET) of nanocatalysts was characterized by N_2 adsorption, and desorption isotherms were obtained at −196 °C using a Quantachrome ChemBET-3000. The thermal stability of the nanocatalysts was determined by TGA analysis. With the PerkinElmer Thermo-gravimetric apparatus, a TGA analysis was performed in flowing air from room temperature to 800 °C at a heating rate of 20 °C/min. To investigate the surface functional groups, Fourier transform infrared spectroscopy (FTIR, UNICAM 4600) was conducted in the range of 400-4,000 cm^{-1} wave numbers. XPS was measured with a Thermo Fisher K-Alpha, equipped with a monochromatic Al Kα X-ray source. Spectra were obtained using aluminium anode (Al Kα=1,486.6 eV) operating at 150 W. Spectra were recorded at background pressure of 2×10^{9} mbar. Binding energies were calibrated using C 1s peak at 284.5 eV.

4. Experimental Setup for Catalytic Performance Test

Fig. 3 shows the experimental setup used for activity measurement of Ni-Cu/Al_2O_3-ZrO_2 nanocatalyst. The test was performed at atmospheric pressure in a 5 mm i.d., U-shape quartz reactor. The amount of loaded nanocatalyst was 0.1 gr and total hydrogen flow rate for reduction of nanocatalysts was 30 ml/min. The reactor was placed in a furnace, which provided the required temperature for catalytic reaction (550 to 850 °C). The feed gas consisted of CO_2 and CH_4 and its flow rate was controlled by MFCs (Beijing Sevenstar Electronics Co Ltd.). Total feed flow rate was set at 40 ml/min during catalytic performance tests. To access the stability test of each nanocatalyst, all tests were carried out for 1,440 min at 850 °C and GHSV (gas hourly space velocity) of 24 *l*/g·h. Both the inlet and the outlet gas concentrations were monitored by means of a gas chromatograph (GC Chrom, Teif Gostar Faraz, Iran), equipped

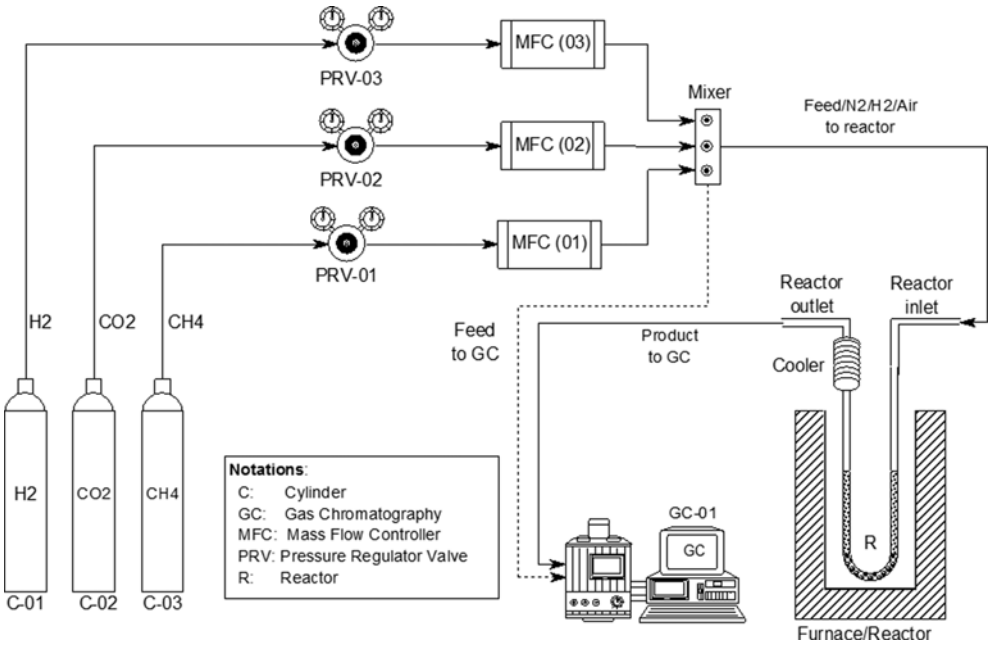

Fig. 3. Experimental setup for catalytic evaluation of Ni-Cu/Al_2O_3 nanocatalyst toward syngas production from reforming of CH_4/CO_2 greenhouse gases.

with TCD and FID detectors, using plot U and Molecular Sieve columns (Agilent Co.) and argon as the carrier gas. The conversion was defined as the CH_4 and CO_2 converted per total amount of CH_4 and CO_2. The yields of CO and H_2 are defined as follows:

$$X_{CH_4}\% = \frac{C_{CH_{4in}} - C_{CH_{4out}}}{C_{CH_{4in}}} \times 100 \quad (6)$$

$$X_{CO_2}\% = \frac{C_{CO_{2in}} - C_{CO_{2out}}}{C_{CO_{2in}}} \times 100 \quad (7)$$

$$Y_{H_2}\% = \frac{C_{H_{2out}}}{2C_{CH_{4in}}} \times 100 \quad (8)$$

$$Y_{CO}\% = \frac{C_{CO_{out}}}{C_{CH_{4in}} + C_{CO_{2in}}} \times 100 \quad (9)$$

where X_i is conversion of reactants and Y_i is yield of products. Ci_{in} is the initial molar fraction of component i in the feed, and Ci_{out} is the final molar fraction of component i in the product stream.

RESULTS AND DISCUSSION

1. Nanocatalyst Characterizations

1-1. XRD Analysis

Fig. 4 illustrates the recorded XRD patterns of γ-alumina support: (a), dried Ni-Cu/Al_2O_3-ZrO_2 nanocatalyst (NCAZ-D) (b), impregnated Ni-Cu/Al_2O_3-ZrO_2 nanocatalyst (NCAZ-I) (c), and plasma-treated Ni-Cu/Al_2O_3-ZrO_2 nanocatalyst (NCAZ-P) (d). All alumina peaks in doped samples shifted to lower 2θ angels, compared to undoped sample. This slight displacement might be due to the formation of $NiAl_2O_4$ spinel. Therefore, doping Ni in all samples (NCAZ-D, NCAZ-I and NCAZ-P) results in formation of $NiAl_2O_4$, which leads to suppression of carbon deposition [34]. The formation of $NiAl_2O_4$ reveals the strong interaction between Ni and Al_2O_3 that

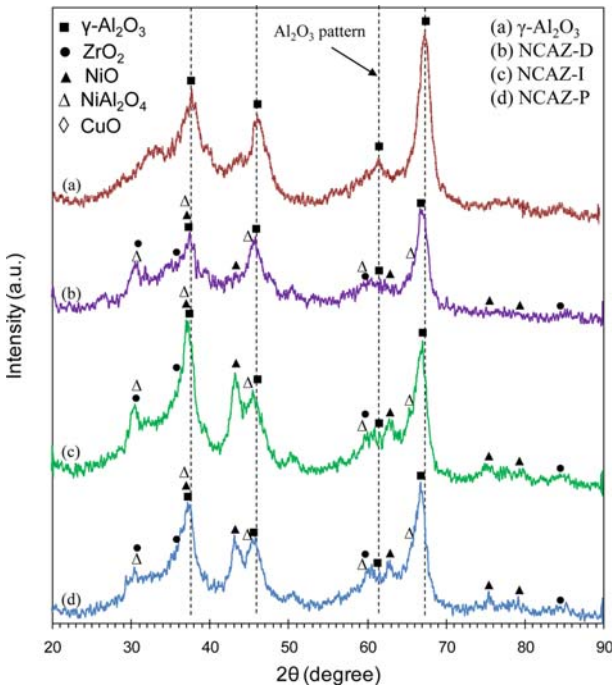

Fig. 4. XRD patterns of (a) γ-Al_2O_3 and Ni-Cu/Al_2O_3-ZrO_2 nanocatalysts: (b) NCAZ-D, (c) NCAZ-I and (d) NCAZ-P.

originates from small Ni crystallites. In fact, small Ni crystallites lead to relatively more resistance toward carbon formation and sintering [35,36]. According to the figure, the existence of Ni as nickel oxide and $NiAl_2O_4$ is revealed. In addition, no characteristic peaks due to the impurities of utilized materials were detected. No characterization peaks attributed to NiO were found in NCAZ-D sample, which shows lack of formation of this compound before thermal treat-

ment. NiO (2θ=37.33, 43.38, 63.02, 75.59 and 79.60) results in weaker peaks for NCAZ-P in comparison with NCAZ-I, showing slightly smaller crystal size and higher dispersion for NiO. The results of the present study show an active phase dispersion enhancement after plasma treatment in the XRD results, which is consistent with the results reported in the literature [37-39]. No reflection due to CuO, Cu_2O or other copper content, was detected in all three samples. This is because copper is present in small quantities and it might be considered as the amorphous state.

1-2. FESEM Analysis

Fig. 5 displays the surface morphology of the plasma-treated and the impregnated Ni-Cu/Al_2O_3-ZrO_2 nanocatalysts. Obvious agglomerated particles were observed in γ-alumina sample. According to FESEM micrographs, the different synthesis methods used in this work produce materials with different morphologies and grain sizes. The particles of NCAZ-I nanocatalyst were large and their surface was comparatively rough. In contrast, spherical particles of NCAZ-P nanocatalyst were small with a uniform dispersion. Although a distinct border between NCAZ-P nanocatalyst particles is not easily visible, large clear agglomerates of particles in NCAZ-I nanocatalyst can be observed. Plasma treatment decreased particle size and plasma high energy species flattened particles on support, increasing the interaction between support and active metals. This comparison indicates the advantage of the plasma method to achieve a better-dispersed matrix compared to that obtained by impregnation method. Fig. 6 shows a surface particle size histogram of the NCAZ-P nanocatalyst. The NCAZ-P has a narrow surface particle size distribution ranging from 8.4 to 58.8 nm. The average surface particle size of NCAZ-P is 18.3 nm, whereas 100% of surface particles are less than 100 nm. As can be seen, more than 51.6% of surface particles have sizes between 10-20 nm.

1-3. TEM Analysis

Fig. 7 shows the TEM micrographs of the plasma-treated Ni-Cu/Al_2O_3-ZrO_2 nanocatalyst (NCAZ-P). From this figure, small particles of active phase are present in the plasma-treated sample. No agglomeration was found and, as it was shown previously in FESEM micrograph of NCAZ-P, all particles are small and well-dispersed. Yu et al. [40] proposed an electronic mechanism to study the effect

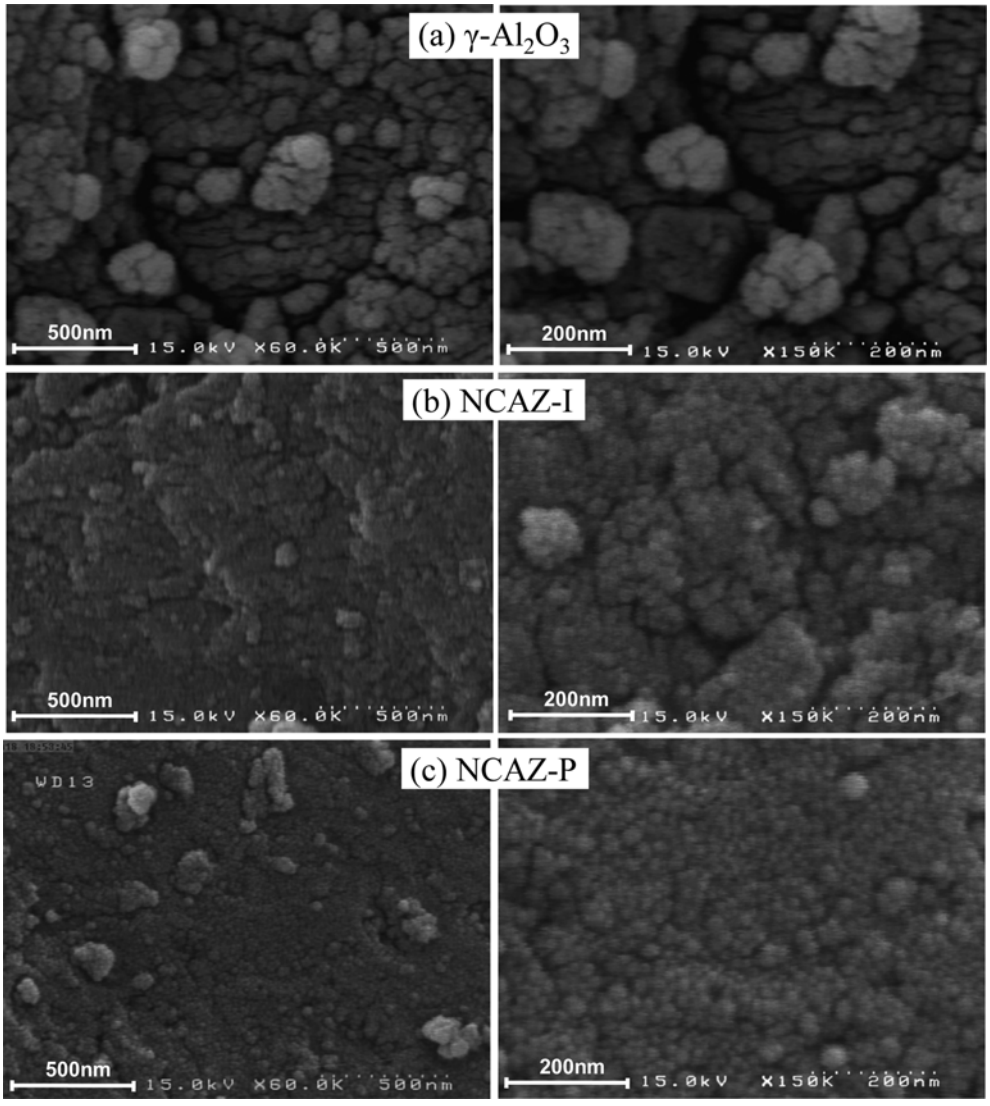

Fig. 5. FESEM images of (a) γ-Al_2O_3 and Ni-Cu/Al_2O_3-ZrO_2 nanocatalysts: (b) NCAZ-D, (c) NCAZ-I and (d) NCAZ-P.

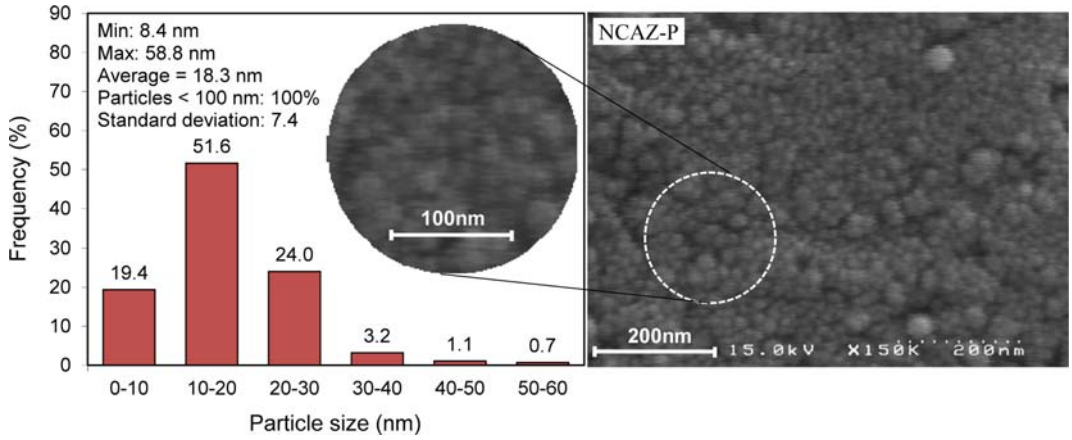

Fig. 6. Surface particle size histogram of Ni-Cu/Al_2O_3-ZrO_2 nanocatalyst treated with non-thermal plasma (NCAZ-P).

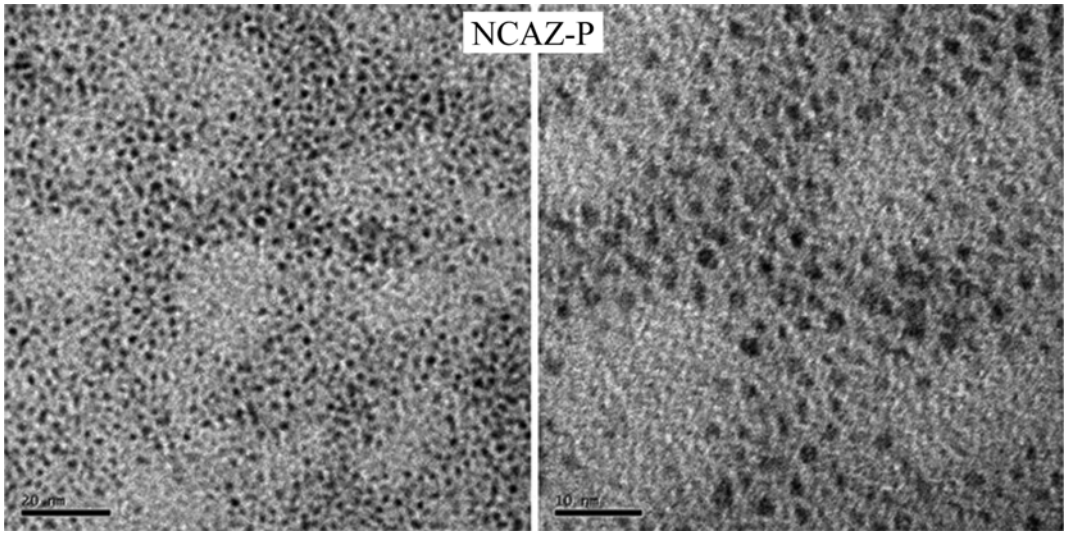

Fig. 7. TEM image of Ni-Cu/Al_2O_3-ZrO_2 nanocatalyst treated with non-thermal plasma (NCAZ-P).

of plasma on nanocatalyst powder. When nanocatalyst powder is exposed to plasma electrons, each particle can trap thousands of electrons [18]. The trapped electrons form a plasma sheath around the particle [41]. While strong Coulomb repulsions exist between these electrons, the electron flow in the plasma field receives a strong repulsive force on the sheath [41]. Under these conditions, the bounds of the precursors or clusters are elongated or distorted and they would be easily split if colliding with other energetic species, resulting in a high dispersion [42] and small catalytic particles. High dispersion of active phase on Al_2O_3-ZrO_2 has a direct effect on nanocatalyst activity and selectivity in CO_2 reforming of methane. Bombardment of nanocatalyst surface by plasma species causes fragmentation in nanocatalyst particles. Moreover, uniformity of plasma environment results in a homogeneous dispersion. Hence, a small and uniform dispersion of Ni particles for NCAZ-P nanocatalyst was obtained. Sietsma et al. showed that a higher metal dispersion was attributed to a more moderate rate of metal nitrate decomposition [43,44]. Glow discharge plasma with a completely gentle decomposition could possibly result in an enhanced Ni and Cu dispersion in NCAZ.

1-4. EDX Analysis

The EDX analysis of the NCAZ-P nanocatalyst is illustrated in Fig. 8. All of the elements used in the synthetic procedure (Ni, Cu, Al and Zr) can be observed in the EDX analysis. From EDX analysis of all these nanocatalysts, good dispersion of Ni and Cu can be concluded. This observation confirms the effect of plasma in improving the dispersion of active phase over support. Plasma has a homogeneous electric field; therefore, homogeneous dispersion of particles occurs in nanocatalyst structure. No sintering or particle agglomeration was observed in NCAZ-P.

1-5. BET Analysis

The BET specic surface area was measured to be 116, 21, 71, and 77 m^2/g for alumina, NCAZ-D and NCAZ-I, and NCAZ-P nanocatalysts, respectively (Fig. 9). The BET surface area of the non calcined sample is very low, indicating the existence of water and precursor residues inside the nanocatalyst pores. It is observed that, after thermal treatment, the surface area of the dried sample increased. This reveals the forming of pore structures with higher surface area during thermal treatment. Small particles synthesized in plasma treatment prevent pore plugging, to some extent, due to gentle decomposition of metal nitrates and homogeneous fragmentation of particles in plasma environment. Therefore, a relatively higher surface area is observed in the case of plasma-treated sample.

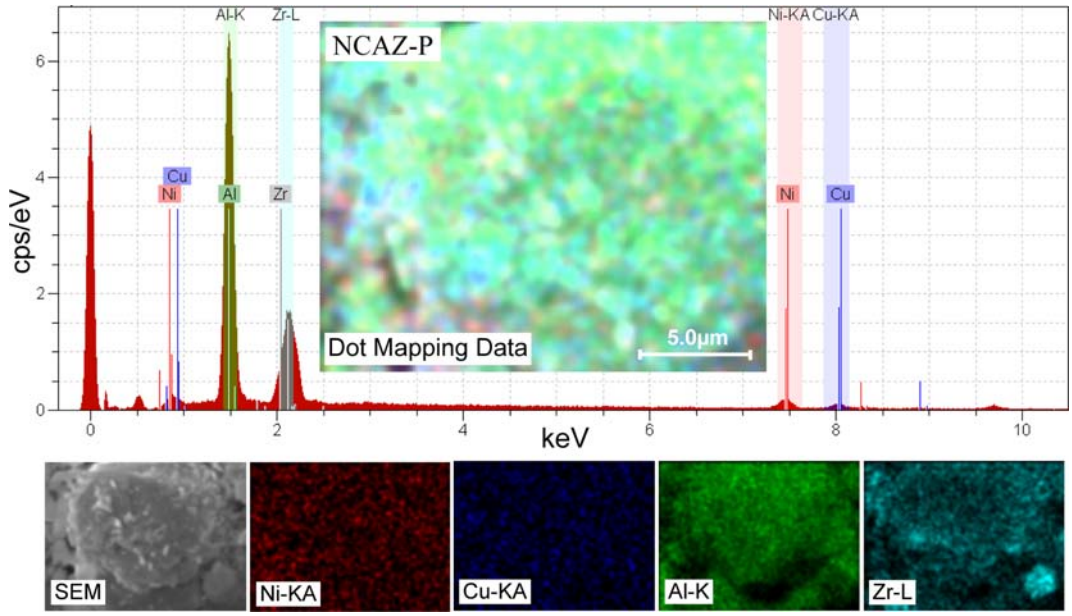

Fig. 8. EDX analysis of Ni-Cu/Al_2O_3-ZrO_2 nanocatalyst treated with non-thermal plasma (NCAZ-P).

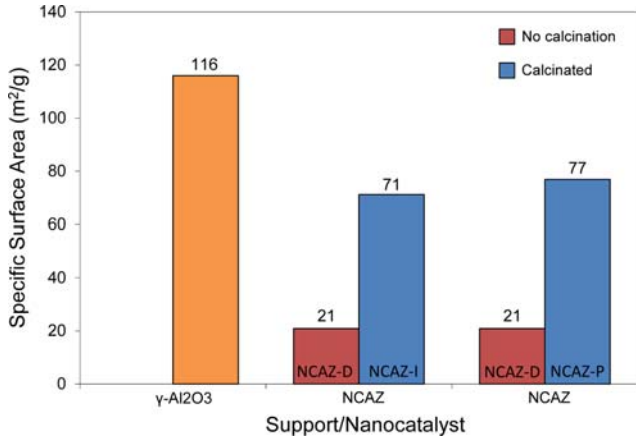

Fig. 9. BET surface area analysis of γ-Al_2O_3 and Ni-Cu/Al_2O_3-ZrO_2 nanocatalysts: NCAZ-D, NCAZ-I and NCAZ-P.

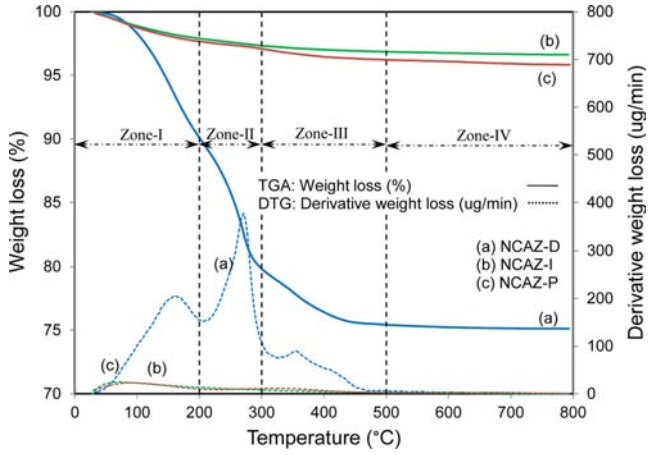

Fig. 10. TG-DTG analysis of Ni-Cu/Al_2O_3-ZrO_2 nanocatalysts: (a) NCAZ-D, (b) NCAZ-I and (c) NCAZ-P.

1-6. TG-DTG Analysis

The TGA and DTG results in Fig. 10 were employed to investigate the changes in thermal state of NCAZ-D, NCAZ-I and NCAZ-P nanocatalysts. The weight loss for NCAZ-I sample is more or less similar to the weight loss of NCAZ-P sample. However, the weight loss for NCAZ-D was very drastic. The weight changes because the thermal treatment can be divided into four zones: 25-200 °C, 200-300 °C, 300-500 °C, and 500 °C. According to Gadalla and Yu's [45] observation, the first and the second zones may result in water desorption from the nanocatalyst structure. This water includes surface water and hydrates inside the metal nitrates. In the temperature range of 300-500 °C, metal hydroxides are converted to metal oxides while above 500 °C no noticeable change is observed in weight of nanocatalysts. It seems that, for NCAZ nanocatalyst, temperatures higher than 500 °C are suitable as the calcination temperature.

1-7. XPS Analysis

The Cu 2p3/2 and Cu 2p1/2 spectra of NCAZ-I and NCAZ-P nanocatalysts are shown in Fig. 11. From the XPS spectra of Cu 2p, the Cu 2p3/2, binding energies at 932.4 eV and 934.3 eV and Cu 2p1/2 at 952.8 eV, could be ascribed to the simultaneous presence of Cu^{2+} and Cu^{+1} in both NCAZ-I and NCAZ-P nanocatalysts. However, XPS spectra indicated that after the plasma treatment more Cu^{+1} was converted to Cu^{+2}. It means that the plasma treatment provides an oxidizing environment to form the most stable form of metallic promoters.

The Cu 2p3/2 and Cu 2p1/2 binding energies of the sample are slightly higher than the data of pure Cu^{+2} and Cu^{+1} reported by Avgouropoulos and Ioannides [46]. According to the previously published papers related to CuO-based nanocatalysts, higher binding energy is possibly caused by the interaction between support and CuO, resulting in the shift of the Cu binding energy [47,48].

According to the calculations, the Cu^{+2}/Al ratio, which represents the CuO dispersion on alumina support, is 5.29 and 9.16 for NCAZ-I and NCAZ-P nanocatalysts, respectively. The Cu^{+2}/Al ratio was

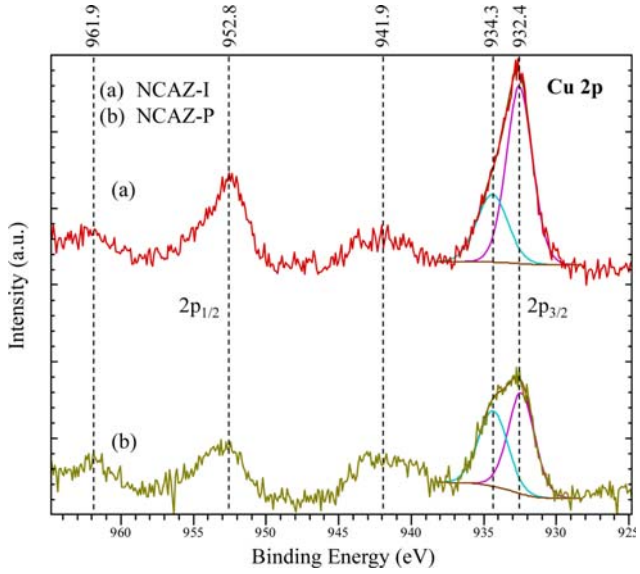

Fig. 11. XPS analysis of Ni-Cu/Al_2O_3-ZrO_2 nanocatalysts: (a) NCAZ-I and (b) NCAZ-P.

higher for NCAZ-P nanocatalysts, showing the best coverage of support by CuO active phase in plasma-treated nanocatalyst. A higher Cu^{+2}/Al means well dispersed CuO particles after plasma treatment, as it was observed in our previous investigations for Ni in plasma-treated Ni/Al_2O_3 nanocatalysts with different promoters [28,30].

1-8. FTIR Analysis

FTIR spectra of γ-Al_2O_3, NCAZ-D, NCAZ-I and NCAZ-P are indicated in Fig. 12. Six main peaks are observed at 530, 710, 1,400, 1,649, 2,370 and 3,450 cm^{-1} in almost all three samples. The impregnated and the plasma-treated nanocatalysts have similar peak positions. Despite the NCAZ-I and NCAZ-P, there is no peak at wave numbers lesser than 1,000 cm^{-1} for γ-Al_2O_3. The absorption peaks below 1,000 cm^{-1} are related to metal oxides (NiO, CuO, Cu_2O) arising from inter-atomic vibrations. There is no metal oxide absorption peak for NCAZ-D sample, showing the lack of formation of metal oxides during drying and the need for a thermal treatment for emerging them. This observation is in a good agreement with the XRD results obtained. For all the investigated materials, there are absorption peaks at 1,400, 1,649 and 3,450 cm^{-1} which can be attributed to the adsorbed water [29,49,50]. The broad peak at 3,450 cm^{-1} has mainly been assigned to interacting OH or to bridging OH groups [51-53]. The peak at 1,649 cm^{-1} is the O-H bending vibrational mode of the interlayer water molecules, which are associated with the adsorbed water on the products [54-56]. The O-H related peaks are similar in plasma-treated and impregnated nanocatalysts; however, they are very intense in the dried sample. The latter reveals the existence of water inside the sample structure and the need for a calcination step. The peak at 2,370 cm^{-1} is associated with the C-H stretching mode of atmospheric hydrocarbons on the surface of the nanocatalysts [57].

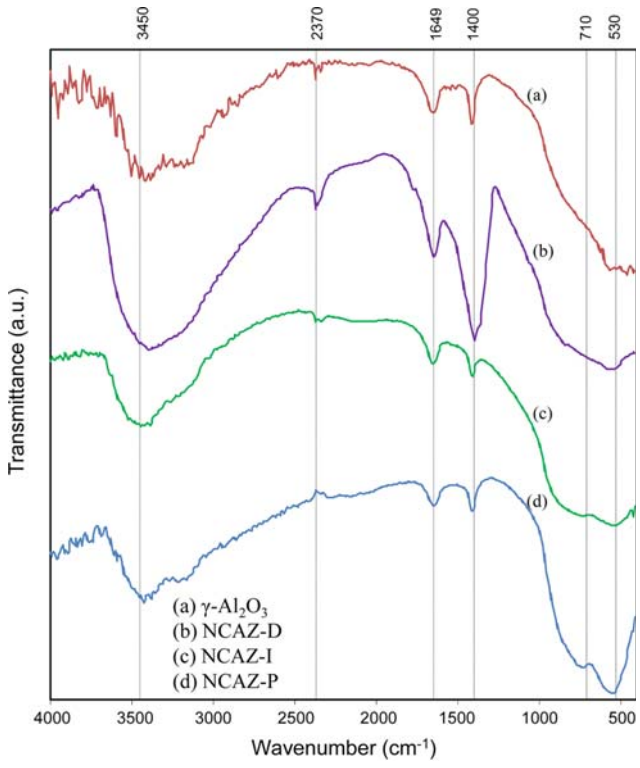

Fig. 12. FTIR spectra of (a) γ-Al_2O_3 and Ni-Cu/Al_2O_3-ZrO_2 nanocatalysts: (b) NCAZ-D, (c) NCAZ-I and (d) NCAZ-P.

2. Catalytic Performance Study toward Reforming of CH_4/CO_2

2-1. Effect of Plasma Treatment

Fig. 13 shows the product yield obtained from both NCAZ-I and NCAZ-P nanocatalysts as a function of temperature. By increasing temperature, the H_2 and CO yields were significantly increased for both samples due to the endothermicity of the reaction. On the other hand, the CO production is higher than the H_2 production for both samples, due to the RWGS reaction [58,59]. Note that the product yield over NCAZ-P is remarkably higher than that over NCA-I, revealing a better activity of plasma-treated nanocatalyst. Using NCAZ-P nanocatalyst, the same yield for CO and H_2 can be obtained at some regions ca. 200 °C lower temperatures. This observation reveals the effect of plasma treatment on the formation of nanoparticles with a better low-temperature activity. According to its intended usage, the rate of H_2/CO is one of the most important parameters of syngas

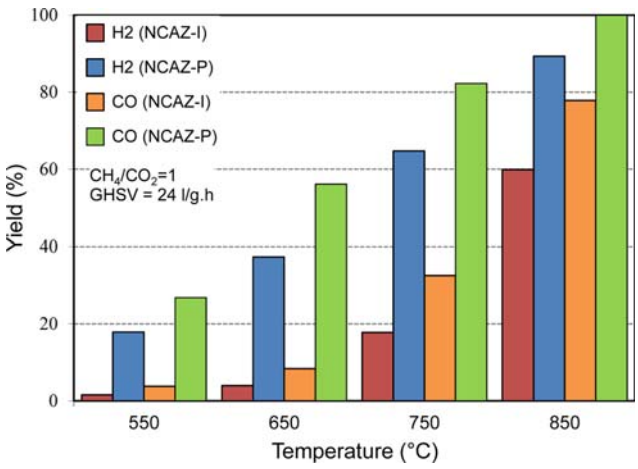

Fig. 13. Effect of temperature on H_2 and CO yields over NCAZ-I and NCAZ-P nanocatalysts.

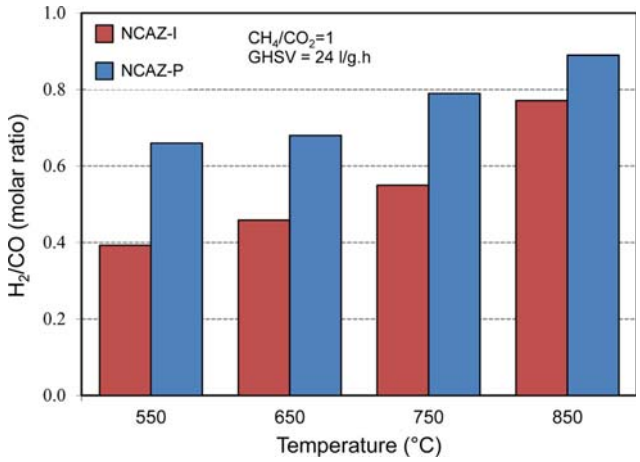

Fig. 14. Effect of temperature on H_2/CO molar ratio produced over NCAZ-I and NCAZ-P nanocatalysts.

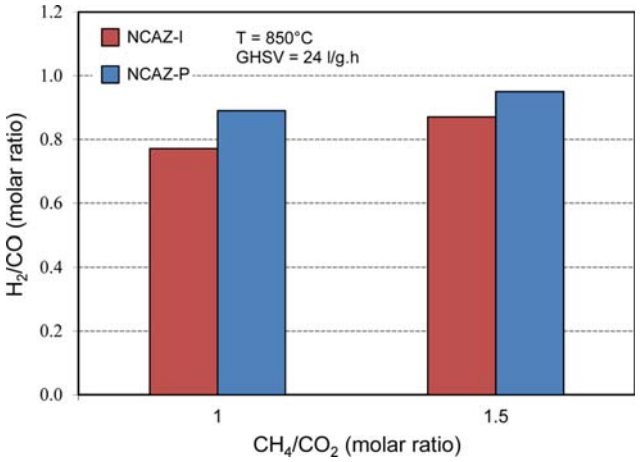

Fig. 16. Effect of CH_4/CO_2 ratio in feed on H_2/CO molar ratio produced over NCAZ-I and NCAZ-P nanocatalysts.

[60].

Investigating the proportion of H_2 to CO is beneficial in understanding the catalytic behavior and the selectivity. This H_2/CO ratio vs. temperature is plotted for both samples in Fig. 14. The H_2/CO ratio is increased by increasing temperature. However, the ratio at all temperatures of the plasma-assisted sample is higher than that at the impregnated sample due to the well-defined structure of plasma-treated nanocatalysts (according to characterization techniques). The H_2/CO<1 was measured for both samples at all reaction temperatures. This observation demonstrates the consumption of hydrogen through RWGS (reaction 2). The H_2/CO ratio gets closer to 1 at higher temperatures and a final value of H_2/CO=0.9 is attained at 850 °C for plasma-treated nanocatalyst. As mentioned earlier, the ratio of H_2/CO=1 is useful for the synthesis of other hydrocarbons and the fuel cell applications.

2-2. Effect of CH_4/CO_2 Ratio in Feed

Fig. 15 illustrates the effect of CH_4/CO_2 ratio on product yield in NCAZ-I and NCAZ-P nanocatalysts. As it is observed, an increase in the CH_4/CO_2 ratio from 1 to 1.5 decreased the H_2 and CO yield in the product stream for both impregnated and plasma-treated nanocatalysts. When the amount of CH_4 in feed is higher than the stoichiometric value, coke formation is more possible [61,62]. Nanocatalyst activity can be affected, and the yield of both H_2 and CO is decreased in the nanocatalysts.

The effect of the feed ratio (CH_4/CO_2) on the H_2/CO ratio over NCAZ-P and NCAZ-I is shown in Fig. 16. The plasma-treated nanocatalyst is more active in producing higher H_2/CO ratios at both studied feed ratios. The H_2/CO ratio increases when CH_4/CO_2 ratio increases from 1 to 1.5. It seems that at higher CH_4/CO_2 ratios, higher amount of H_2 are produced due to the reaction (5).

2-3. Effect of GHSV

The effect of GHSV on CH_4 and CO_2 conversion and product yield for NCAZ-I and NCAZ-P nanocatalysts is illustrated in Fig. 17 and Fig. 18, respectively. The CH_4 and CO_2 conversions and H_2/CO yield decrease as GHSV increases in both the impregnated and the plasma-treated nanocatalysts. Different explanations could be presented for this observation. A decrease in both CH_4 and CO_2 conversions and H_2/CO yield was observed by Mark and Maier [62] due to the external diffusion resistance at high GHSVs. Basini and Sanlippo [64] claimed that the decrease in CH_4 and CO_2 conversions is attributed to the reverse reactions such as CO hydrogenation to CH_4 at high GHSVs. According to our observations, more

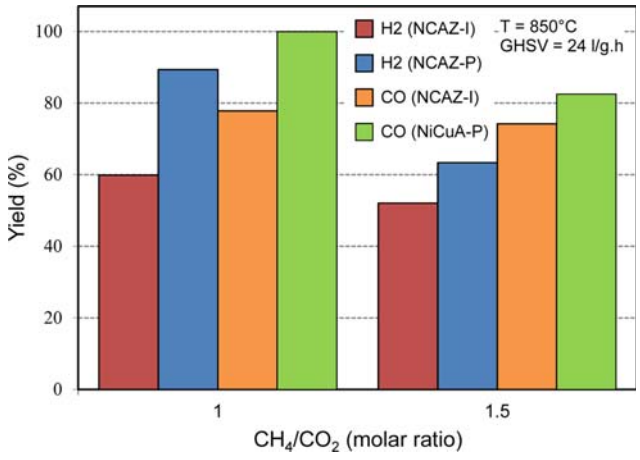

Fig. 15. Effect of CH_4/CO_2 ratio in feed on H_2 and CO yields produced over NCAZ-I and NCAZ-P nanocatalysts.

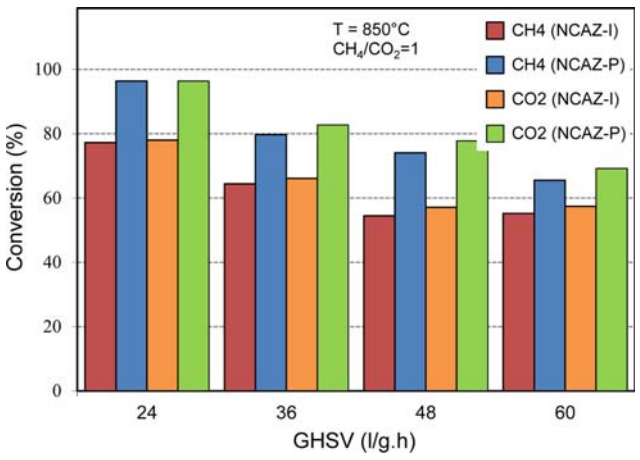

Fig. 17. Effect of GHSV on CH_4 and CO_2 conversions over NCAZ-I and NCAZ-P nanocatalysts.

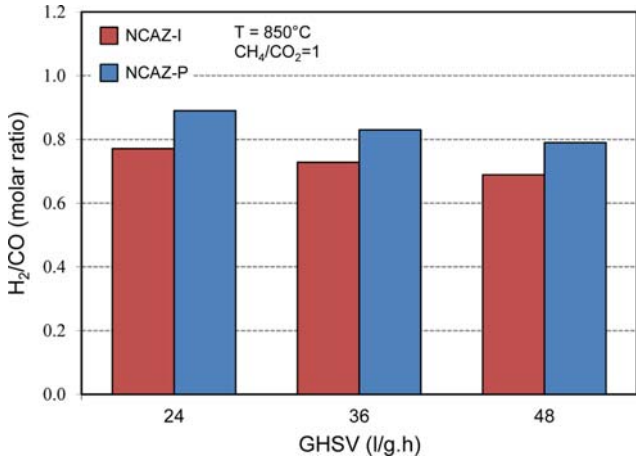

Fig. 18. Effect of GHSV on H_2/CO molar ratio produced over NCAZ-I and NCAZ-P nanocatalysts.

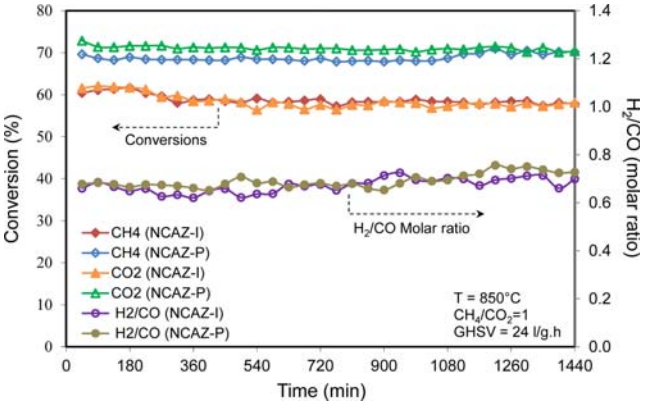

Fig. 19. Time on stream performance of NCAZ-I and NCAZ-P nanocatalysts in terms of CH_4 and CO_2 conversions.

GHSV means lesser contacting time; therefore, the reactants have less opportunity to diffuse in nanocatalyst pores.

According to its intended usage, the rate of H_2/CO is one of the most important parameters of syngas. With increasing GHSV, this value goes far from 1, showing that the optimal conditions have not been achieved. The latter reveals the consumption of hydrogen through RWGS at higher GHSVs.

2-4. Time on Stream Performance

The NCAZ-I and NCAZ-P samples were tested for 1,440 min time on stream at 850 °C and CH_4. The CO_2 conversions and the produced H_2/CO changes vs. time are shown in Fig. 19. Both NCAZ-I and NCAZ-P nanocatalysts did not reveal deactivation in terms of CH_4 and CO_2 conversion as well as H_2/CO ratio. In CO_2 reforming of methane, carbon is possibly produced from reactions (3) and (4). At high temperatures, methane decomposition (reaction (4)) is thermodynamically favored, but reaction (3) leading to consume carbon. It seems that in the both nanocatalysts, there is a balance between these two types of reactions. It is known that the metals like Cu inhibit carbon deposition over nanocatalyst via controlling the size of Ni ensembles [65]. Furthermore, the oxidation of coke produced from reaction (4) occurs over ZrO_2 which guarantees stability of the both nanocatalysts.

CONCLUSIONS

The present investigation confirms that the plasma treatment can lead to the production of Ni-Cu/Al_2O_3-ZrO_2 nanocatalyst with smaller particles, better dispersion of active phase, higher surface area and uniform morphology. Moreover, plasma treatment induces an enrichment of active phase species on the alumina-zirconia surface that influences better catalytic activities of plasma-treated nanocatalyst. The plasma-treated Ni-Cu/Al_2O_3-ZrO_2 nanocatalyst showed good stability, lower temperature activity, higher H_2/CO ratio and higher yield of H_2 and CO in CO_2 reforming of methane in comparison with those obtained using impregnated nanocatalyst.

ACKNOWLEDGEMENTS

The authors gratefully acknowledge National Iranian Oil Refining and Distribution Company for the financial support of the research under project number of 87-1037 as well as Sahand University of Technology and Iran Nanotechnology Initiative Council for complementary financial supports.

REFERENCES

1. R. Benrabaa, A. Löfberg, A. Rubbens, E. Bordes-Richard, R. N. Vannier and A. Barama, *Catal. Today*, **203**, 188 (2013).
2. P. Estifaee, M. Haghighi, N. Mohammadi and F. Rahmani, *Ultrason. Sonochem.*, **21**, 1155 (2014).
3. C. Fukuhara, R. Hyodo, K. Yamamoto, K. Masuda and R. Watanabe, *Appl. Catal. A: Gen.*, **468**, 18 (2013).
4. T. H. Gardner, J. J. Spivey, E. L. Kugler and D. Pakhare, *Appl. Catal. A: Gen.*, **455**, 129 (2013).
5. S. M. Sajjadi, M. Haghighi and F. Rahmani, *J. Sol. Gel. Sci. Technol.*, **70**, 111 (2014).
6. Y. Vafaeian, M. Haghighi and S. Aghamohammadi, *Energy Convers. Manage.*, **76**, 1093 (2013).
7. N. Wang, X. Yu, Y. Wang, W. Chu and M. Liu, *Catal. Today*, **212**, 98 (2013).
8. Y. H. Hu and E. Ruckenstein, *Advances in catalysis*, Academic Press, 297 (2004).
9. J. R. H. Ross, *Catal. Today*, **100**, 151 (2005).
10. S. Aghamohammadi, M. Haghighi and S. Karimipour, *J. Nanosci. Nanotechnol.*, **13**, 4872 (2013).
11. S. M. Sajjadi, M. Haghighi, A. Alizadeh Eslami and F. Rahmani, *J. Sol.-Gel. Sci. Technol.*, **67**, 601 (2013).
12. X. Zhang, W.-j. Sun and W. Chu, *J. Fuel Chem. Technol.*, **41**, 96 (2013).
13. B. Fidalgo, L. Zubizarreta, J. M. Bermudez, A. Arenillas and J. A. Menendez, *Fuel Process. Technol.*, **91**, 765 (2010).
14. A. Horvath, G. Stefler, O. Geszti, A. Kienneman, A. Pietraszek and L. Guczi, *Catal. Today*, **169**, 102 (2011).
15. A. Y. Khodakov, W. Chu and P. Fongarland, *Chem. Rev.*, **107** 1692 (2007).
16. D.-g. Cheng, Q. Xia and C. j. Liu, *Studies in surface science and catalysis*, 33 (2004).
17. M. Zhang, D.-g. Cheng and Y.-p. Zhang, *Preprints of Papers-American Chemical Society, Division of Fuel Chemistry*, **49**, 188 (2004).

18. J. J. Zou, C. J. Liu and Y. P. Zhang, *Langmuir*, **22**, 2334 (2006).
19. A. Golebiowski, K. Stołecki, U. Prokop, A. Kucœmierowska, T. Borowiecki, A. Denis and C. Sikorska, *React. Kinet. Catal. Lett.*, **82**, 179 (2004).
20. K. Nagaoka, A. Jentys and J. A. Lercher, *J. Catal.*, **229**, 185 (2005).
21. J.-S. Chang, S.-E. Park and H. Chon, *Appl. Catal. A: Gen.*, **145**, 111 (1996).
22. F. Frusteri, F. Arena, G. Calogero, T. Torre and A. Parmaliana, *Catal. Commun.*, **2**, 49 (2001).
23. Z. Hou, O. Yokota, T. Tanaka and T. Yashima, *Appl. Catal. A: Gen.*, **253**, 381 (2003).
24. A. A. Lemonidou, M. A. Goula and I. A. Vasalos, *Catal. Today*, **46**, 175 (1998).
25. J.-S. Choi, K.-I. Moon, Y. Kim, J. Lee, C.-H. Kim and D. Trimm, *Catal. Lett.*, **52**, 43 (1998).
26. X. Dong, X. Cai, Y. Song and W. Lin, *J. Natural Gas Chem.*, **16**, 31 (2007).
27. N. Rahemi, M. Haghighi, A. A. Babaluo, M. Fallah Jafari and S. Allahyari, *Catal. Sci. Technol.*, **3**, 3183 (2013).
28. N. Rahemi, M. Haghighi, A. A. Babaluo, M. Fallah Jafari and P. Estifaee, *J. Nanosci. Nanotechnol*., **13**, 4896 (2013).
29. P. Estifaee, M. Haghighi, A. A. Babaluo, N. Rahemi and M. F. Jafari, *J. Power Sources*, **257**, 364 (2014).
30. N. Rahemi, M. Haghighi, A. A. Babaluo, M. Fallah Jafari and P. Estifaee, *Plasma Chem. Plasma Process.*, **33**, 663 (2013).
31. N. Rahemi, M. Haghighi, A. A. Babaluo, M. Jafari Fallah and P. Estifaee, *J. Ind. Eng. Chem.*, **19**, 1566 (2013).
32. N. Rahemi, M. Haghighi, A. A. Babaluo, M. F. Jafari and S. Khorram, *J. Appl. Phys.*, **114**, 094301 (2013).
33. N. Rahemi, M. Haghighi, A. A. Babaluo, M. F. Jafari and S. Khorram, *Int. J. Hydrog. Energy*, **38**, 16048 (2013).
34. Y.-g. Chen and J. Ren, *Catal. Lett.*, **29**, 39 (1994).
35. H. S. Bengaard, J. K. Nørskov, J. Sehested, B. S. Clausen, L. P. Nielsen, A. M. Molenbroek and J. R. Rostrup-Nielsen, *J. Catal.*, **209**, 365 (2002).
36. B. S. Liu and C. T. Au, *Appl. Catal. A: Gen.*, **244**, 181 (2003).
37. C.-j. Liu, K. Yu, Y.-p. Zhang, X. Zhu, F. He and B. Eliasson, *Appl. Catal. B: Environ.*, **47**, 95 (2004).
38. G. Liu, Y. Li, W. Chu, X. Shi, X. Dai and Y. Yin, *Catal. Commun.*, **9**, 1087 (2008).
39. Y.-P. Zhang, P.-S., Ma, X. Zhu, C.-J. Liu. and Y. Shen, *Catal. Commun.*, **5**, 35 (2004).
40. K. L. Yu, C. J. Liu, Y. P. Zhang, F. He, X. L. Zhu and B. Eliasson, *Plasma Chem. Plasma Process.*, **24**, 393 (2004).
41. Z.-j. Wang, Y. Zhao, L. Cui, H. Du, P. Yao and C.-j. Liu, *Green Chem.*, **9**, 554 (2007).
42. J. Kaspar, P. Fornasiero and M. Graziani, *Catal. Today*, **50**, 285 (1999).
43. J. R. A. Sietsma, H. Friedrich, A. Broersma, M. Versluijs-Helder, A. Jos van Dillen, P. E. de Jongh and K. P. de Jong, *J. Catal.*, **260**, 227 (2008).
44. J. R. A. Sietsma, J. D. Meeldijk, J. P. Den Breejen, M. Versluijs-Helder, A. J. Van Dillen, P. E. De Jongh and K. P. De Jong, *Angew. Chem.*, **46**, 4547 (2007).
45. A. M. Gadalla and H. F. Yu, *J. Therm. Anal.*, **37**, 319 (1991).
46. G. Avgouropoulos and T. Ioannides, *Appl. Catal. A: Gen.*, **244**, 155 (2003).
47. Y.-Z. Chen, B.-J. Liaw and H.-C. Chen, *Int. J. Hydrog. Energy*, **31**, 427 (2006).
48. J. Huang, S. Wang, Y. Zhao, X. Wang, S. Wang, S. Wu, S. Zhang and W. Huang, *Catal. Commun.*, **7**, 1029 (2006).
49. M. Parvas, M. Haghighi and S. Allahyari, *Environ. Technol.*, **35**, 1140 (2014).
50. F. Rahmani, M. Haghighi and P. Estifaee, *Micropor. Mesopor. Mater.*, **185**, 213 (2014).
51. S. Aghamohammadi, M. Haghighi and M. Charghand, *Mater. Res. Bull.*, **50**, 462 (2014).
52. S. Allahyari, M. Haghighi, A. Ebadi and S. Hosseinzadeh, *Ultrason. Sonochem.*, **21**, 663 (2014).
53. M. Ebrahimynejad, M. Haghighi and N. Asgari, *J. Nanoscience and Nanotechnol.*, **14**, 6848 (2014).
54. N. Asgari, M. Haghighi and S. Shafiei, *J. Chem. Technol. Biotechnol.*, **88**, 690 (2013).
55. Z. Jamalzadeh, M. Haghighi and N. Asgari, *Front. Environ. Sci. Eng.*, **7**, 365 (2013).
56. R. Khoshbin, M. Haghighi and N. Asgari, *Mater. Res. Bull.*, **48**, 767 (2013).
57. K. Anandan and V. Rajendran, *Mater. Sci. Semicond. Process.*, **14**, 43 (2011).
58. F. F. de Sousa, H. S. A. de Sousa, A. C. Oliveira, M. C. C. Junior, A. P. Ayala, E. B. Barros, B. C. Viana, J. M. Filho and A. C. Oliveira, *Int. J. Hydrog. Energy*, **37**, 3201 (2012).
59. J. Zhang, H. Wang and A. K. Dalai, *Appl. Catal. A: Gen.*, **339**, 121 (2008).
60. M. Haghighi, Z.-q. Sun, J.-h. Wu, J. Bromly, H. L. Wee, E. Ng, Y. Wang and D.-k. Zhang, *Proceedings of the Combustion Institute*, **31**, 1983 (2007).
61. J. H. Edwards and A. M. Maitra, *Fuel Process. Technol.*, **42**, 269 (1995).
62. A. M. Gadalla and B. Bower, *Chem. Eng. Sci.*, **43**, 3049 (1988).
63. M. F. Mark and W. F. Maier, *J. Catal.*, **164**, 122 (1996).
64. L. Basini and D. Sanfilippo, *J. Catal.*, **157**, 162 (1995).
65. S. Zhang, J. Wang, H. Liu and X. Wang, *Catal. Commun.*, **9**, 995 (2008).